Dislocation-induced changes in quantum dots: step alignment and radiative emission.

R. Leon, J. O. Okuno and R. A. Lawton
Jet Propulsion Laboratory, California Institute of Technology, 4800 Oak Grove Drive, Pasadena, CA 91109

M. Stevens-Kalceff and M. R. Phillips
Microstructural Analysis Unit, University of Technology, Sydney, NSW 2007, Australia

J. Zou and D. J. H. Cockayne
Australian Key Centre for Microscopy and Microanalysis, The University of Sydney, NSW 2006, Australia

C. Lobo
EME, Research School of Physical Sciences and Engineering, Australian National University, Canberra, ACT 0200, Australia

ABSTRACT

A transition between two types of **step alignment** was observed in a multilayered **InGaAs/GaAs quantum-dot** (QD) structure. A change to larger QD sizes in smaller concentrations occurred after formation of a **dislocation array**. Cathodoluminescence (CL) spectra show a bimodal peak with lower energy peak enhancement when probing at lower e-beam energies. The two peaks separate as a result of QD interdiffusion. CL imaging and cross-sectional transmission electron microscopy showed contrast from a dislocation array formed at the interface between GaAs and the first InGaAs QD layer. Strong QD emission in the near infrared (800 to 1100 nm) was obtained despite the presence of dislocations.

PACS: 85.30.Vw, 68.55.-a, 78.60.Hk, 81.15.Gh

There is considerable interest in multilayered quantum dot (QD) structures to increase gain in QD lasers and to achieve better spatial ordering in self-forming QDs. Buried strain fields from preformed islands induce vertical alignment in closely stacked QD layers [1,2]. An added bonus is the observation of narrower photoluminescence (PL) lines in vertically aligned InAs/GaAs [2,3] and InP/InGaP [4] QDs.

Besides vertical alignment, increased ordering within planes has been predicted [5] and experimentally demonstrated [5,6], making multilayer structures particularly promising. Recent experiments confirm increased spatial ordering; however, surface roughening is also seen after growth of a few QD layers in Ge/Si and InAs/GaAs. Combining self-organization and photolithography has recently shown to give very narrow inhomogeneous PL lines [7]. Other types of alignment are observed in non-patterned structures. These include bunched island strings at multi-atomic steps [8,9], and alignment via dislocation array slip plane interaction in Ge/Si islands [10]. Ordered array formation is also seen in metallic island nucleation as in Ni on Au (111) [11]. These are all promising strategies to induce periodic nanostructure formation.

Issues to consider in using dislocation arrays to nucleate III-V QDs include possible effects of dislocations on QD radiative recombination. A recent study of the optical evolution of InGaAs QD formation found a sharp drop in luminescence intensity [12] associated with an increase in the concentration of incoherent islands, suggesting the latter to be optically inactive. However, dislocations do not seem to strongly affect the optical properties of InAs quantum dots on GaAs/Si substrates [13]. These apparently contradictory findings may be understood by considering differences in emission from incoherent islands and from coherent islands found near a misfit dislocation network.

In this work we discuss a new type of QD alignment for an InGaAs/GaAs QD multilayered structure. QDs show a transition between two types of alignment at different stages of the growth, from step edge alignment along [010] to counter step alignment (along [100]). These and other structural changes were found after formation of a dislocation network at the

InGaAs/GaAs interface. We observed strong radiative emission from QDs, even after formation of a dislocation array.

InGaAs islands were formed by metalorganic chemical vapor deposition in a horizontal reactor operating at 76 Torr. After growth of a GaAs buffer layer (100 nm) at 650°C, the temperature was lowered to 550°C and a 100-layered structure composed of alternating nanometer-size InGaAs islands and thin GaAs layers were formed by depositing 5 MLs of $In_{0.6}Ga_{0.4}As$ and 10 nm GaAs on semi-insulating GaAs (001) with 2° miscut towards [101] (steps along [010]). Part of the structure was also treated by post-growth rapid thermal annealing at 950 C for 60 seconds using proximity capping in Argon. Atomic force microscopy (AFM) with etched silicon nitride tips and Scanning Electron Microscopy (SEM) gave statistics on island sizes and areal densities. Cross-section Transmission Electron Microscopy (TEM) specimens were prepared using standard ion milling and dimpling techniques. TEM specimens were investigated in a Phillips EM 430 operating at 300 keV. Cathodoluminescence (CL) was carried out in a JEOL JSM35C scanning electron microscope with a liquid He cold stage and a monochromater/mirror, and the signal collected with a liquid N_2 cooled Ge detector and lock-in techniques.

Figure 1 shows the result of deposition of one layer of InGaAs islands or QDs on vicinal (100) GaAs. The QDs and surface steps are clearly seen, with islands forming "strings" along multi-atomic step edges. As seen in previous studies [9], nucleation on steps is energetically favorable. Figure 1 (b) and (c) show the surface morphology after growth of 100 InGaAs/GaAs QD layers. The islands exhibit a stronger alignment, but the alignment is now normal to the step direction, while still appearing to nucleate on steps. Another feature apparent from Figs 1(b) and 1(c) is the morphological change in the steps themselves. Undulations are seen, the steps appear discontinuous, and with greater average separation. Detailed AFM also show greater step bunching than after growth of a single layer of QDs. Increase in QD size and decreases in their concentration seem concurrent with the changes in QD alignment. Analysis of AFM images give estimated average diameters of 38 nm and concentrations of 6 x $10^9/cm^2$ for the dots formed on

the first layer, and 75 nm and 1.3 x $10^8/cm^2$ for average diameters and concentrations in the last layer. Aspect ratios between island heights and radii are roughly constant (~ 1/4) for both types of islands.

The depth resolved behavior of the bimodal CL peak shown in Fig. 2 was investigated by varying the electron beam energy, while maintaining constant beam power. Two distinct Gaussian peaks (dotted line in Fig. 2) contribute to the CL spectra and their relative intensities change as a function of electron range. The relatively broad FWHM arise from the electron beam averaging over large ensembles of QDs with slightly different sizes. Selective excitation of a small number of QDs can resolve this broad peak into ultra-sharp emission lines [14,15]. The behavior of the bimodal CL peak with varying excitation conditions is in agreement with our structural data. The contribution from the low energy peak is larger at low beam energy, since electron hole pairs are formed closer to the surface, thereby collecting a greater portion of the signal from the larger QDs. The relative intensities of the two convoluted peaks are seen to change with electron beam penetration depth, and at 15 keV beam energy the integrated intensity of the high-energy peak is greater. From Wojs et al [16], ground state emission energies for lens-shaped InGaAs/GaAs QDs are 1.26 eV and 1.20 eV for QDs of 38 nm and 75 nm diameters respectively. These are in good agreement with our values from fits to the experimental data [1.266 ± .0090 and 1.196 ± .0015 eV].

The last spectrum in Fig 2 shows the effects of intermixing or interdiffusion on our multi-layered structure. As found in earlier studies, interfacial compositional disordering in InGaAs/GaAs QDs causes strong blue shifts in ground state emission and narrower inhomogeneous luminescence peaks [17]. It has also been shown that these blue shifts depend on QD size and dots/barrier materials composition [17, 18]. Here both peaks show a strong blue shift, but of different magnitudes. The 1.266 eV peak originating from the smaller QDs shifts more, therefore the peaks separate completely with interdifussion. It can also be seen that interdiffusion here affects the two types of QDs very differently. The higher energy peak narrows considerably, while maintaining the same integrated intensity as the original peak. The lower

energy peak shifts slightly less, and its integrated intensity is much reduced compared with the original peak (15 keV curve in figure 2). Part of these differences can be explained by varying surface conditions. For the larger dots near the surface, the QD layers range 10 to 900 nm from the surface. This might explain the different peak shape, since interdiffusion in the first and last layers is occurring under very different condition. The smaller QDs are 900 to 1000 nm from the surface, so the conditions are more homogeneous. Previous studies in intermixed coherent QDs have shown that intermixing does not have a detrimental effect on the low temperature PL intensity [17]. The loss in intensity of the first peak might indicate a less stable microstructure after interdiffusion.

Figure 3 shows cross-sectional TEM images of this structure. Figure 4 (a) shows the entire (~ 1 μm thick) multilayer structure. The misfit dislocation array shows at the interface between the GaAs buffer layer and the first InGaAs QD plane. Orthogonal dislocations are seen when tilting the TEM specimen, so that the array is inclined to the electron beam [Figure 4 (b)].

The effective critical thickness can be estimated using theoretical predictions [19] and experimental observations [20]. Considering an average or effective Indium composition over each QD layer plus GaAs spacer layers to be x= 0.067, the critical thickness ($\mathbf{t}_c$) is: $25 < \mathbf{t}_c \leq 45$ nm. The experimental value will be closer to the upper limit, and the island formation will give some strain relaxation, which will increase the effective $\mathbf{t}_c$ even further. This will give at least 4 dislocation free layers (QDs and GaAs spacers), so we expect formation of a misfit dislocation array at or after the fifth QD layer.

The QDs realign with increasing number of deposited layers. For a few layers, the QDs form along [010] surface steps. At $\mathbf{t}_c$, interfacial dislocations form along <110>. Unlike in previous findings for the Ge/Si system [10], this alignment is seen along the [101] direction. In III-V semiconductors, α misfit dislocations (which lie along [1-10]) form preferentially over the β dislocations (along [110]). However, in miscut stepped surfaces, mixed behaviors can be seen [21]. The mechanism by which dislocations mediate island nucleation is still unclear. If the larger QDs nucleate after formation of 5-10 layers of the smaller QDs, it seems unlikely that their

ordering is triggered directly by the strain field from the dislocations, because these are too far from the area of island nucleation (50 to 100 nm away).

The increase in QD size and decrease in their concentration with further deposition of QD layers is seen after formation of the dislocation array. The strain in the film is reduced due to plastic deformation. The natural length scale associated with strain driven islanding is proportional to $\Delta\Gamma/M\varepsilon^2$, where $\Delta\Gamma$ is the change in surface energy, **M** is the elastic modulus and ε is the lattice mismatch strain. When dislocations are introduced, there is an effective change in ε and larger islands could be formed because of lower effective mismatch [22]. This abrupt change in effective ε is the most likely explanation for the increase in island sizes after formation of the dislocation array. From this argument and the depth dependent results from CL, we believe that the changes in island size are simultaneous with formation of the dislocation array.

In conclusion, we have shown two distinct types of InGaAs dot alignment in vicinal GaAs (001). An abrupt transition in QD sizes and concentrations was also seen. These results also show bright QD emission despite formation of a dislocation array and different behaviors with thermal intermixing.

Part of this work was started at the Australian National University, sponsored by the Australian Research Council and was completed at the Jet Propulsion Laboratory, California Institute of Technology, under a contract with the National Aeronautics and Space Administration.

REFERENCES

1. Q. Xie, A. Madhukar, P. Chen, and N. P. Kobayashi, *Phys. Rev. Lett.* **75**, 2542 (1995).
2. G. S. Solomon, J.A. Trezza, A. F. Marshall, and J. S. Harris Jr., *Phys. Rev. Lett.* **76**, 952 (1996).
3. Y. Sugiyama, Y. Nakata, K. Imamura, S. Muto, and N. Yokoyama, *Jap. J. App. Phys.* **35**, 1320 (1996).
4. M. K. Zundel, P. Specht, K. Eberl, N. Y. Jin-Phillipp and F. Phillipp, *Appl. Phys. Lett.* **71**, 2972 (1997).
5. J. Tersoff, C. Teichert and M. G. Lagally, *Phys. Rev. Lett.* **76**, 1675 (1996).
6. G. S. Solomon, S. Komarov, J.S. Harris Jr., and Y. Yamamoto, *J. Cryst. Growth* **175-176**, 707 (1997).
7. R. Notzel, Z. Niu, M. Ramsteiner, H.-P. Schonherr, A. Tranpert, L. Daweritz and K. H. Ploog, Nature **392**, 56 (1998)
8. N. Ikoma and S. Ohkouchi, *Jpn. J. Appl. Phys.* **34**, L724 (1995).
9. R. Leon, T. J. Senden, Yong Kim, C. Jagadish, and A. Clark, *Phys. Rev. Lett* **78**, 4942 (1997).
10. S. Yu. Shiryaev, F. Jensen, J. L. Hansen, J. W. Petersen, and A. N. Larsen, *Phys. Rev. Lett.* **78**, 503 (1997).
11. D. D. Chambliss, R. J. Wilson and S. Chiang, *Phys. Rev. Lett* **66**, 1721 (1991).
12. R. Leon and S. Fafard, *Phys. Rev. B* **58**, R1726 (1998).
13. J. M. Gerard, O. Cabrol, and B. Sermage, *Appl. Phys. Lett.* **68**, 3123 (1996).
14. S. Fafard, R. Leon, D. Leonard, J.L. Merz, and P.M. Petroff, *Phys Rev B* **50**, R8086 (1994).
15. R. Leon, P. M. Petroff, D. Leonard, and S. Fafard, *Science* **267**, 1966 (1995).
16. A. Wojs, P. Hawrylak, S. Fafard and L. Jacak, *Phys. Rev. B* **54**, 5604 (1996).
17. R. Leon, D. R. M. Williams, J. Krueger, E. R. Weber and M. R. Melloch, *Phys. Rev. B* **56**, R4336 (1997).
18. C. Lobo, R. Leon, S. Fafard and P.G. Piva, *Appl. Phys. Lett.* **72**, 2850 (1998).
19. J. W. Matthews and A. E. Blakeslee, J. Cryst. Growth 27, 118 (1974).
20. J. Zou, D. J. H. Cockayne, and B. F. Usher, J. Appl. Phys. 73, 619 (1993).
21. R. S. Goldman, K. L. Kavanagh, H. Wieder, S. Ehrlich, and R. M. Feenstra, J. Appl. Phys. 83, 5137 (1998).
22. J. A. Floro, G. A. Lucadamo, E. Chason, L. B. Freund, M. Sinclair, R. D. Twesten, and R. Q. Hwang, *Phys. Rev. Lett.* **80**, 4717 (1998).

FIGURE CAPTIONS

Figure 1. Initial and final surface morphologies of a structure containing 100 layers of InGaAs QDs. (a) Deflection AFM micrograph of structure after the first layer deposition showing preferential alignment along steps [[100] direction]. (b) SEM micrograph of surface structure after 100 layers deposition. (c) AFM surface plot showing step alignment detail from (b).

Figure 2. CL spectra at different accelerating potentials give different average penetration depths of electron hole pair formation as shown in the inset schematic at 7, 9 and 15 keV. Calculated ranges in GaAs are 0.34, 0.52 and 1.22 μm respectively. Gaussian fits was obtained with two peaks centered at 1.197 and 1.265 eV with 54.4 and 60 meV broadening for the 7 keV curve; 1.196 and 1.257 eV with 54.4 and 71.5 meV broadening in the 9 keV curve, and 1.194 and 1.275 eV with 53.9 and 73.5 meV broadening for 15 keV. Integrated intensity ratios [low energy/high energy peaks] are 1.56, 0.71 and 0.65 for the spectra at 7, 9 and 15 keV respectively. The lowest spectrum (15 keV beam energy) shows the results of intermixing (annealing at 950 C for 60 sec).

Figure 3. Bright-field images of a [110] cross section TEM sample, showing (a) misfit dislocation(s) lying at the bottom interface and (b) a misfit dislocation network for a tilted sample (~ 50 degree along 220* reflections).

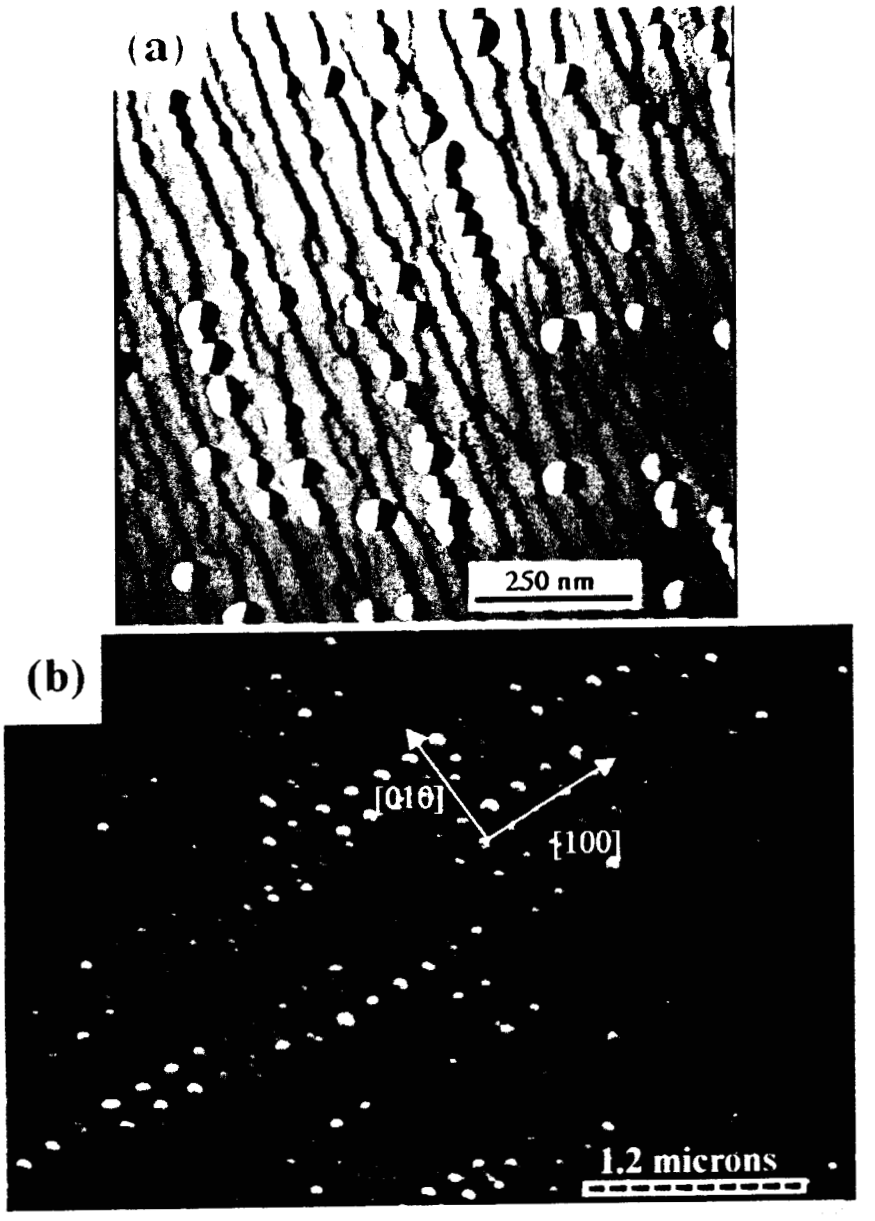

Fig 1, R. Leon, AP-

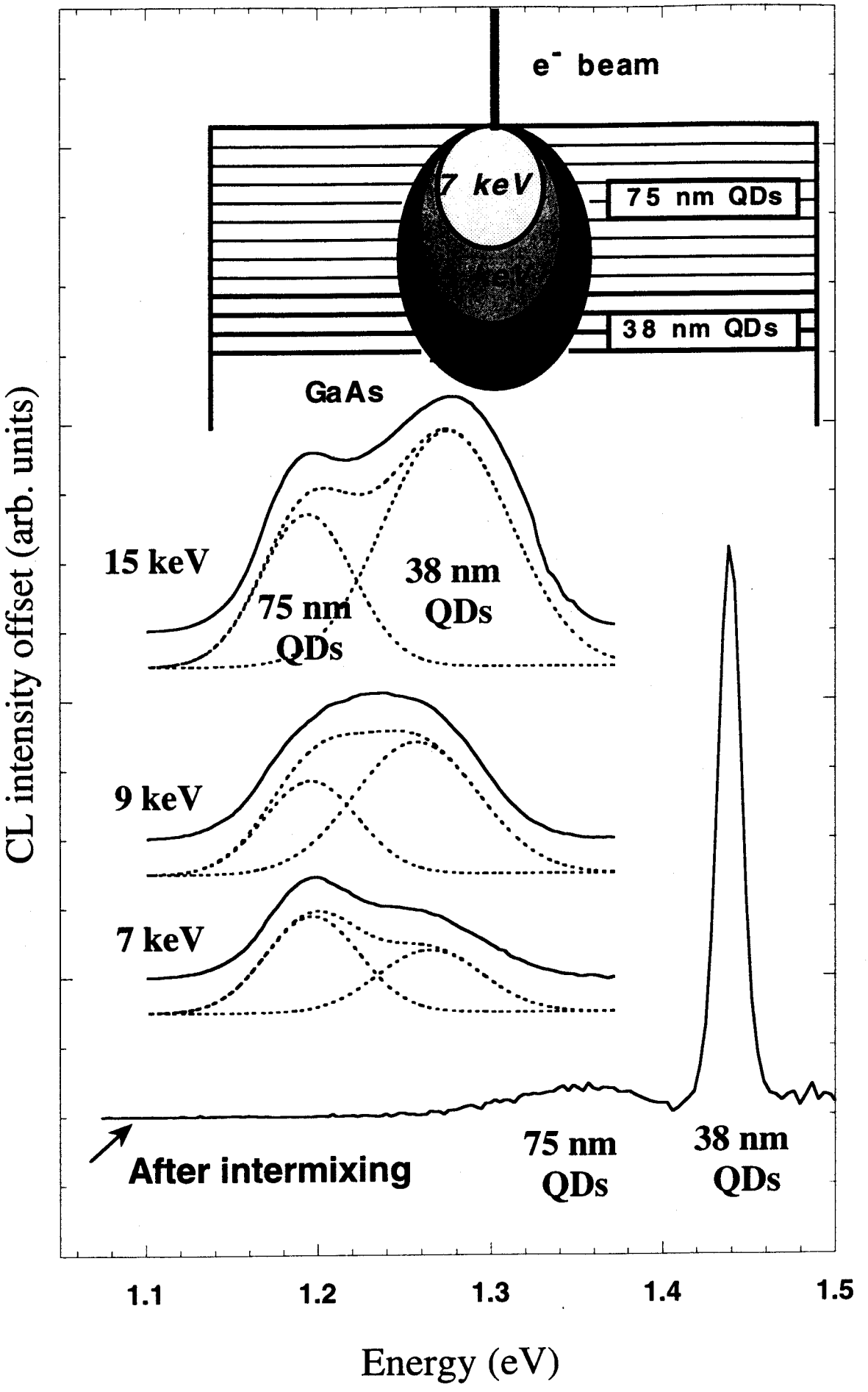
e⁻ beam
7 keV
75 nm QDs
38 nm QDs
GaAs
15 keV
75 nm QDs
38 nm QDs
9 keV
7 keV
After intermixing
75 nm QDs
38 nm QDs
CL intensity offset (arb. units)
1.1
1.2
1.3
1.4
1.5
Energy (eV)

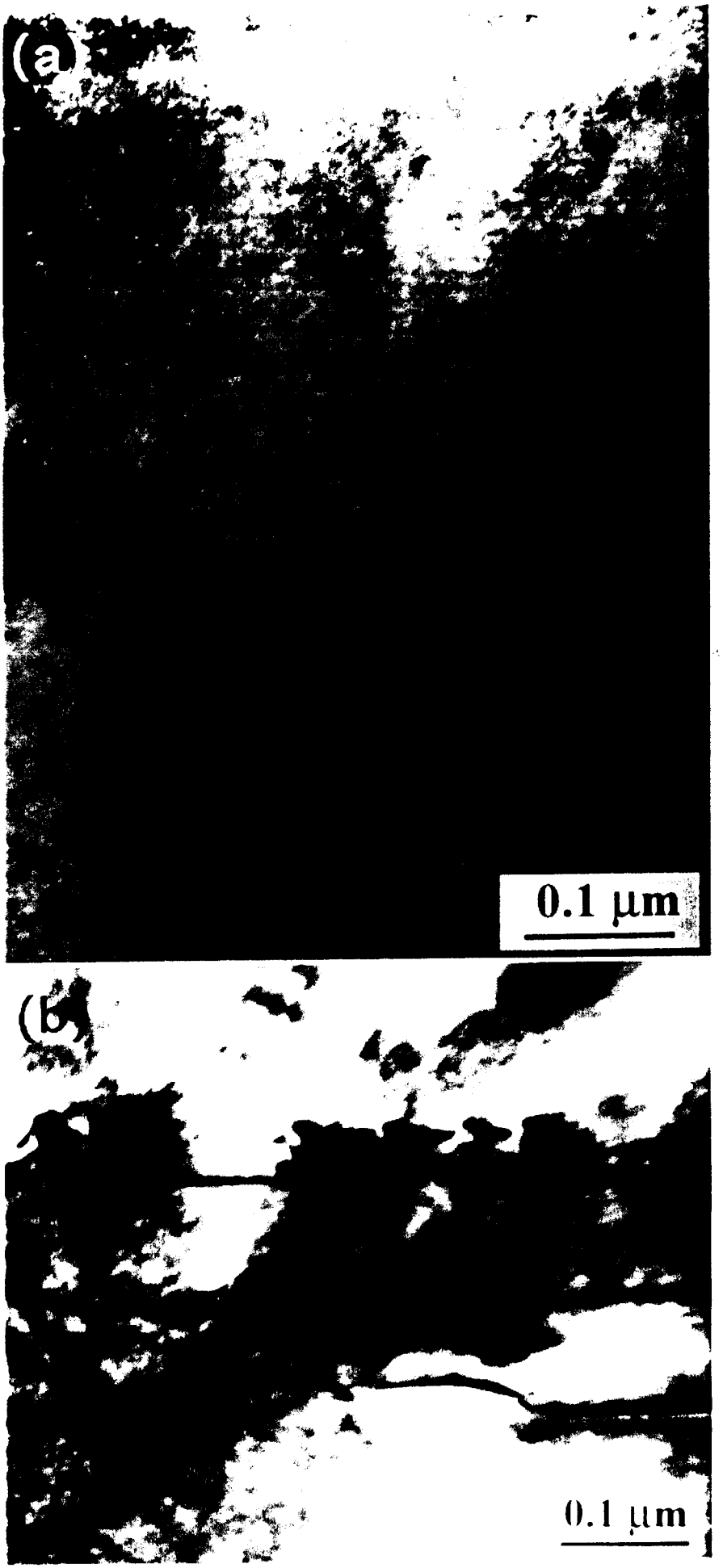

Fig 3 Rileam, A